



Oxygen vacancy promoted CO oxidation over Pt/CeO₂ catalysts: A reaction at Pt–CeO₂ interface

Huan-Huan Liu, Yu Wang, Ai-Pin Jia, Shu-Yuan Wang, Meng-Fei Luo, Ji-Qing Lu*

Key Laboratory of the Ministry of Education for Advanced Catalysis Materials, Institute of Physical Chemistry, Zhejiang Normal University, Jinhua 321004, China

ARTICLE INFO

Article history:

Received 29 May 2014

Received in revised form 30 June 2014

Accepted 30 June 2014

Available online 7 July 2014

Keywords:

CO oxidation

Pt/CeO₂ catalysts

Interfacial reaction

Oxygen vacancy

Kinetic study

ABSTRACT

A series of Pt/CeO₂ catalysts with different Pt contents were prepared using an incipient wetness impregnation method and tested for CO oxidation. Kinetic study on the catalysts indicated that the reaction rate was independent of the partial pressures of CO and O₂ ($r = k_{app}[CO]^0[O_2]^0$). The derived reaction pathways involved chemisorption of CO on surface Pt atoms and reacting with lattice oxygen provided by the CeO₂ support at the Pt–CeO₂ interface, suggesting a Mars van-Krevelen type reaction on these catalysts and the interfacial Pt–O–Ce ensembles being the active sites. Also, turnover frequencies (TOFs) calculated based on Pt dispersion and periphery Pt atoms were found to be proportional to the Pt particle size, with the large Pt particles possessing higher TOF than the small ones. Such a trend was interpreted by the important role of the oxygen vacancies via the formation of Pt–Ce–O solid solution, which could accelerate the mobility of lattice oxygen and consequently the activity.

© 2014 Elsevier B.V. All rights reserved.

1. Introduction

CO oxidation is a very important topic in catalysis because of its wide practical applications in indoor air cleaning, CO gas sensors, CO₂ lasers and automotive exhaust treatment [1,2]. Besides, such a “simple” reaction is highly valuable in understanding many fundamental concepts in catalysis.

Noble metals such as Au [3,4], Pd [5] and Pt [6,1,7] have been extensively investigated for CO oxidation. In spite of continuous efforts, understanding of this reaction remains ambiguous. One issue is the structure sensitivity. For the Au catalysts, it is commonly agreed that CO oxidation is extremely structure sensitive, with small Au nanoparticles possessing higher activities than the large ones [3]. However, for the Pt catalysts, situation seems more complicated and somehow contradictory. Although it has been recognized that the supported Pt catalysts show less structure sensitivity or structure insensitivity [8–11], it was also reported that the turnover frequencies (TOFs) decreased with increasing Pt dispersion [12] over Pt/SiO₂ catalysts (larger Pt particles were more active than the smaller ones) or the TOFs decreased with increasing Pt particle sizes over Pt/TiO₂ catalysts [13]. Another puzzling issue is the reaction mechanism of CO oxidation over Pt catalysts. Various elementary steps have been proposed in literature

[9,12–14]. These reaction models include competitive or non-competitive chemisorption of O₂ and CO on Pt surface, interfacial reaction between CO chemisorbed on Pt atoms and O₂ chemisorbed on the reducible support, and the participation of lattice oxygen in the reaction (Mars van-Krevelen model). As a result, different rate equations and activation energies (30–150 kJ mol^{−1}) were reported [15]. For example, the rate expressions had a dependency of −1 on CO partial pressure and a dependency of 1 on O₂ partial pressure over Pt/Al₂O₃ catalysts ($r = k[CO]^{-1}[O_2]$) [9,15], while our recent work on Pt/TiO₂ catalysts established a rate equation of $r = k[CO]^{0.29}[O_2]^{0.19}$ [13]. Moreover, on Pt/CeO₂ catalysts [16], it was reported that the rate expression was independent of either CO or O₂ partial pressure ($r = k[CO]^0[O_2]^0$).

It is realized that the behaviors of Pt catalysts for CO oxidation are related to multiple parameters such as the morphologies of the Pt nanoparticles (differently coordinated Pt atoms), the pretreatment conditions (pre-oxidation or pre-reduction of the catalyst), reaction conditions (oxygen lean or oxygen rich environment) and the support (inert support or reducible oxides). These parameters are often inter-crossed during the reaction and thus make the catalytic behaviors differ from various Pt catalysts. In order to better understand the reaction mechanism, kinetic investigation is a powerful tool, by which rate expression and possible reaction pathways could be derived. Besides, the particle size effect should be analyzed based on proper reaction models. For example, turnover frequencies (TOFs) are often used to compare the intrinsic activities of different catalysts, which are usually calculated based on

* Corresponding author. Tel.: +86 579 82287325; fax: +86 579 82282595.

E-mail address: [jinqinglu@zjnu.cn](mailto:jiqinglu@zjnu.cn) (J.-Q. Lu).



metal dispersion in the catalyst. Such a correlation is true when all the surface metal atoms participate in the reaction (i.e. on Pt single crystals or Pt supported on inert oxides such as SiO_2 or Al_2O_3); however, it has been proved that when metals are supported on reducible oxides such as TiO_2 , Fe_2O_3 , CeO_2 and MnO_2 , CO oxidation occurs at the metal-support interface, which has been evidenced on various catalyst systems such as Au/TiO_2 [17–19], Pt/TiO_2 [13], CuO/CeO_2 [20,21] and CuO/MnO_2 [22] catalysts. In this case, correlation between the TOF concerning periphery metal atoms and metal particle diameter seems more adequate to reflect size dependency because only the metal atoms located at the periphery of metal-support interface are the reacting sites (the other surface metal atoms serve as collection zone).

Therefore, in this work, CO oxidation was conducted over a series of Pt/CeO_2 catalysts to investigate the kinetics and the effect of Pt particle size on the reaction. Under rigorously controlled reaction conditions, rate expressions on these catalysts were obtained in kinetic region and elementary steps were proposed which fit well with the kinetic results. Extra attention was also paid on the support, as CeO_2 is a well-known “active” oxide which plays important role in the activation of oxygen species particularly in oxidation reactions [23]. It was found that the presence of oxygen vacancies in the CeO_2 could remarkably affect the observed activities.

2. Experimental

2.1. Catalyst preparation

The CeO_2 support was prepared using a sol-gel method. $\text{Ce}(\text{NO}_3)_3 \cdot 6\text{H}_2\text{O}$ and citric acid with a molar ratio of 1/2 was dissolved in distilled water and the mixed solution was continuously stirred at 90 °C until a gel was obtained. The solid was then dried at 120 °C overnight, followed by calcination at 500 °C for 4 h.

Supported Pt catalysts were prepared using an incipient wetness impregnation method. In a typical procedure, an appropriate amount of aqueous solution of $\text{Pt}(\text{NO}_3)_2$ (Shanghai Jiuyue Chemical Ltd., 99.9%) was added to 2 g of the CeO_2 support, and the mixture was kept for 4 h. Then it was mildly evaporated at 90 °C and dried at 120 °C overnight. Finally, the solid was calcined at 400 °C for 3 h. The catalysts were designated $x\text{Pt}/\text{CeO}_2$, as the x referred to the weight percent of Pt (wt.%) in the catalyst.

2.2. Catalyst characterizations

The BET surface areas of the catalysts were measured by N_2 adsorption at liquid-nitrogen temperature (77 K), using a surface area analyzer (Quantachrome Autosorb-1). The catalysts were pretreated at 120 °C for 6 h in vacuum.

X-ray diffraction (XRD) patterns were recorded using a PANalytic X'Pert PW3040 diffractometer with Cu K α radiation operating at 40 kV and 40 mA. The patterns were collected in a 2 θ range from 10° to 90°, with a scanning step of 0.15°/s. The crystallite sizes and cell parameters of the catalysts were analyzed using the JADE 6.5 software.

Actual contents of Pt in the catalysts were determined by X-ray fluorescence (XRF) analysis, on an ARL ADVANT'X Intelli Power 4200 scanning X-ray fluorescence spectrometer. The results were analyzed using UniQuant non-standard sample quantitative analysis software.

CO chemisorption experiments were carried out on a Quantachrome CHEMBET-3000 instrument in order to determine the dispersion of Pt. The Pt/CeO_2 catalyst was placed in a U-shaped quartz reactor and a high-purity He (99.999%) gas flow of 70 ml min⁻¹ was used as the carrier gas. Before CO chemisorption, the samples were reduced in a H_2-N_2 mixture (5 vol.% H_2) stream at

300 °C for 1 h, cooled down to 30 °C, and then purged with a pure He gas flow (30 ml min⁻¹) for 1 h at the same temperature. Then pulses of CO were fed into the stream of carrier gas with a precision analytical syringe. The dispersion of Pt in the catalyst was calculated based on the assumption that $\text{CO:Pt}_{\text{surface}} = 1:1$. And the particle size of Pt was calculated according to the equation $d_{\text{Pt}} (\text{nm}) = 1.1/D$.

The reduction properties of the samples were measured by hydrogen temperature-programmed reduction ($\text{H}_2\text{-TPR}$) experiments. The Pt/CeO_2 catalyst was placed in a quartz reactor, and then heated from room temperature to 800 °C at a rate of 10 °C min⁻¹ in a H_2-N_2 gas (5 vol.% H_2 , 30 ml min⁻¹). The hydrogen consumption during the reduction was determined by a gas chromatograph with a thermal conductivity detector (TCD). The water produced in TPR was trapped on a 5 Å molecular sieve.

X-ray photoelectron spectra (XPS) were recorded using a VG ESCALAB MK-2 spectrometer with Al K α radiation (1486.6 eV). The voltage and power for the measurements were 12.5 kV and 250 W, respectively. The vacuum in the test chamber during the collection of spectra was kept at 2×10^{-8} Pa. The spectra obtained, once the background was removed, were fitted to Lorentzian and Gaussian lines to obtain the number of components, peak position, and their areas. The adventitious C 1 s line at 284.6 eV was used as an internal standard. Before the measurement, the samples were in situ pretreated using an O_2/Ar mixture (10% O_2 in Ar, 30 ml min⁻¹) at 300 °C for 0.5 h, followed by a H_2/Ar mixture (10% H_2 in Ar, 30 ml min⁻¹) at 300 °C for 0.5 h.

Raman spectra were recorded on a Renishaw RM1000 with a confocal microprobe Raman system using an excitation laser line of 514 nm, in a range from 100 to 1800 cm⁻¹.

In situ Fourier transform infrared (FTIR) spectra of the samples were recorded on a NEXUS670 spectrometer equipped with a MCT detector. A self-supported wafer (diameter = 16 mm) was prepared from 30 mg of sample by pressing at about 3 MPa. The sample was transferred to a quartz IR cell connected to the closed circulation systems. The sample was pretreated under a pure O_2 flow (30 ml min⁻¹) at 300 °C for 0.5 h, followed by a pure H_2 flow (30 ml min⁻¹) at 300 °C for another 0.5 h. The sample was then purged by a pure He (30 ml min⁻¹) and cooled down to 40 °C, followed by the background spectrum collection. After that, a pure CO flow (30 ml min⁻¹) was introduced to the sample until a saturated CO chemisorption was obtained. Then the sample was purged by pure He to remove the gas phase and physisorbed CO molecules and a spectrum was collected. Temperature-dependent FTIR spectra during the reaction were recorded after holding each temperature point for 10 min.

2.3. Catalytic testing

Catalytic CO oxidation was performed on a tubular quartz micro reactor (6 mm i.d.) using catalyst with size of 0.12–0.15 mm. Different weight of the catalyst was employed in order to control the CO conversion at low levels (typically below 20% at low reaction temperatures (<60 °C) to ensure a differential reaction mode). The catalyst was diluted with quartz sand in the same mesh size to 0.25 ml. Prior to reaction, the sample was pretreated with an O_2/Ar mixture (10% O_2 in Ar, 30 ml min⁻¹) at 300 °C for 0.5 h, followed by a H_2/Ar mixture (10% H_2 in Ar, 30 ml min⁻¹) at 300 °C for 0.5 h. After the pretreatment, the sample was cooled down to certain temperature and a feed gas consisting of 1% CO and 1% O_2 in N_2 was introduced. The total flow rate was 40 ml (NTP) min⁻¹, corresponding to a space velocity (S.V.) of 9600 h⁻¹. The reaction temperature was monitored by a thermocouple placed in the middle of the catalyst bed. The CO concentration in the reactor effluent was analyzed using an Agilent 6850 gas chromatograph equipped with a TCD detector attached to an HP PLOT column (30 m × 0.32 mm × 12 μm).

Concerning the intrinsic activity, two types of turnover frequencies (TOFs) were calculated based on the following definitions:

$$\text{TOF}_a(s^{-1}) = X_{\text{CO}} F_{\text{CO}} \frac{M_{\text{Pt}}}{(m_{\text{cat}} X_{\text{Pt}} D_{\text{Pt}})}$$

where X_{CO} is the CO conversion at certain temperature; F_{CO} is the flow rate of CO in unit of mol s^{-1} ; m_{Cat} is the amount of catalyst; X_{Pt} is the Pt loading in the catalyst; D_{Pt} is the dispersion of Pt; M_{Pt} is the molar weight of Pt ($195.08 \text{ g mol}^{-1}$). TOF_a reflects the conventional calculation of turnover frequency based on the metal dispersion.

$$\text{TOF}_b(s^{-1}) = X_{\text{CO}} F_{\text{CO}} N_{\text{AV}} \frac{m_{\text{Pt,c}}}{(m_{\text{cat}} X_{\text{Pt}})} \frac{1}{3.6\pi d}$$

where X_{CO} is the CO conversion at certain temperature; F_{CO} is the flow rate of CO in unit of mol s^{-1} ; N_{AV} is the Avogadro's constant; m_{Cat} is the amount of catalyst; X_{Pt} is the Pt loading in the catalyst; $m_{\text{Pt,c}}$ means the weight of a single Pt crystallite depending on its size, which could be derived from its volume obtained under the assumption of its semi-spherical shape and density of Pt (21.35 g cm^{-3}). d is the crystallite size of Pt. 3.6 is the average site density of Pt atoms on the periphery, calculated by $1/d_{(\text{Pt-Pt})}$, where $d_{(\text{Pt-Pt})}$ is the distance of Pt–Pt bond (0.2775 nm). TOF_b reflects the turnover frequency based on the metal sites located on the Pt–CeO₂ interface.

2.4. Reaction kinetics

The kinetic study was performed on the same fixed bed reactor of the catalytic CO oxidation as mentioned above. The feed gases were measured with mass flow controllers and mixed prior to the reactor inlet. For kinetic measurements, the reactor was operated in a differential mode with CO conversion less than 15%. The reaction conversion was controlled by changing the load of catalyst, which was diluted with quartz sand to a volume of 0.1 ml. The diluted catalyst was embedded with glass wool on both sides. A thermocouple was inserted into the middle of the catalyst bed to monitor the reaction temperature. Also, the absence of mass transport resistances was also checked by Weisz–Prater criterion for internal diffusion and Mears' criterion for external diffusion and the absence of heat transfer was checked by Mears' criterion [24] (See Supplementary Information for detailed calculation). For the 2.0Pt/CeO₂ catalyst, the calculated values under kinetic conditions are 1.16×10^{-3} for the Weisz–Prater criterion for internal diffusion, 2.14×10^{-3} for the Mears' criterion for external diffusion and 0.03 for the Mears' criterion for heat transfer. Those results ensure plug-flow and isothermal conditions within the catalyst bed. Partial pressure dependencies of the reaction rates were measured by adjusting the flow rate of 10% CO/Ar or 10% O₂/Ar, while keeping the total flow rate at 120 ml min^{-1} by adjusting the flow rate of pure Ar. In this kinetic experiment, the concentration of CO or O₂ in the feed was varied between 0.1 and 3%. Each measurement was taken after stable rate was achieved, which took about 1 h. CO₂ concentration in the outlet gas stream was also analyzed by the same Agilent 6850 gas chromatograph mentioned above. Conversion of CO was calculated as follows:

$$X_{\text{CO}} = \frac{[\text{CO}]_{\text{in vol.\%}} - [\text{CO}]_{\text{out vol.\%}}}{[\text{CO}]_{\text{in vol.\%}}} \quad (1)$$

where $[\text{CO}]_{\text{in}}$ and $[\text{CO}]_{\text{out}}$ were the CO concentrations in the inlet and outlet gas (vol.%) respectively. And the X_{CO} was used to calculate the reaction rate as follows:

$$r_{\text{CO}} = \frac{N_{\text{CO}} \cdot X_{\text{CO}}}{W_{\text{cat}}} \quad (2)$$

where N_{CO} is the CO molar gas flow rate in mol s^{-1} , W_{cat} is the catalyst weight in grams, r_{CO} is the reaction rate in $\text{mol}_{\text{CO}} \text{ g}_{\text{cat}}^{-1} \text{ s}^{-1}$.

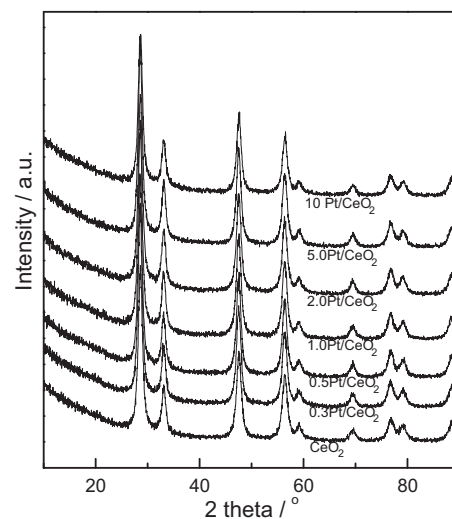


Fig. 1. XRD patterns of Pt/CeO₂ catalysts.

The power-rate law expressions were obtained by taking partial pressure of each reactant (KPa) and the reaction rate data and simultaneously fitting the entire data set by linear least squares regression analysis using the POLYMATH 5.1 program [25].

3. Results and discussion

3.1. Characterizations of Pt/CeO₂ catalysts

The prepared Pt/CeO₂ catalysts have surface areas of $31\text{--}48 \text{ m}^2 \text{ g}^{-1}$, with the high Pt-content sample possessing higher surface area than the low Pt-content one (Table 1). Also, the actual Pt contents are very close to the nominal values (Table 1). In addition, Pt dispersions in the catalysts measured by CO chemisorption progressively decline with increasing Pt loadings, from 0.98 for the 0.3Pt/CeO₂ to 0.15 for the 10Pt/CeO₂. Accordingly, the Pt particle sizes of the catalysts were estimated, ranging from 1.2 to 7.5 nm, as summarized in Table 1. These values suggest the growth of Pt particles in the catalysts with increasing Pt content.

Fig. 1 shows the XRD patterns of the Pt/CeO₂ catalysts. Characteristic diffraction peaks at 2θ of 28.6, 33.1, 47.6, 56.4, 59.3, 69.6, 76.9, 79.3 and 88.6° are observed in all the catalysts, corresponding to a typical cubic CeO₂ phase (JCPDS PDF# 34-0394). However, no diffraction peaks due to metallic Pt⁰ or Pt oxides could be detected, probably due to the fact that Pt species are highly dispersed on the support. The XRD results are quite consistent with the CO chemisorption results, excepted for the two high Pt-loading samples (5.0Pt/CeO₂ and 10Pt/CeO₂). In addition, crystallite sizes of CeO₂ in these catalysts are estimated to be about 11 nm, as listed in Table 1. Analyses of lattice parameter reveal that the values gradually decline with increasing Pt content in the catalyst (Table 1). For example, the pure CeO₂ support has a lattice parameter of 0.54109 nm, while the 10Pt/CeO₂ sample has a lattice parameter of 0.54091 nm. The lowered values in the Pt-containing samples indicate that partial Pt species penetrate in the CeO₂ matrix to form Ce–Pt–O solid solution, because the ionic radius of Pt²⁺ (0.074 nm) or Pt⁴⁺ (0.076 nm) is smaller than that of Ce⁴⁺ (0.097 nm) and the replacement of Ce⁴⁺ by Pt^{2+/4+} will result in the shrinkage of the CeO₂ cell. Moreover, the lattice parameter declines with increasing Pt content in the catalyst, implying more Ce–Pt–O solid solution is formed in the high Pt-loading catalyst.

The morphologies of the catalysts were analyzed by TEM, as shown in Fig. S1 (Fig. S1 in Supplementary Information). The presence of Pt and PtO_x species in the catalysts is evidenced by the

Table 1Physical properties of various Pt/CeO₂ catalysts.

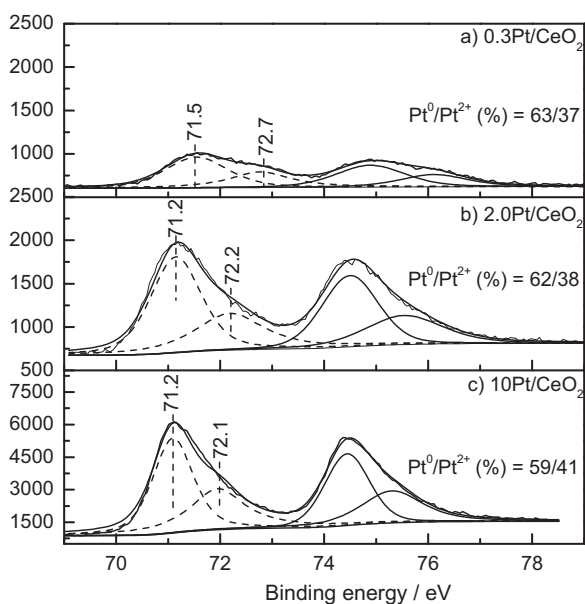
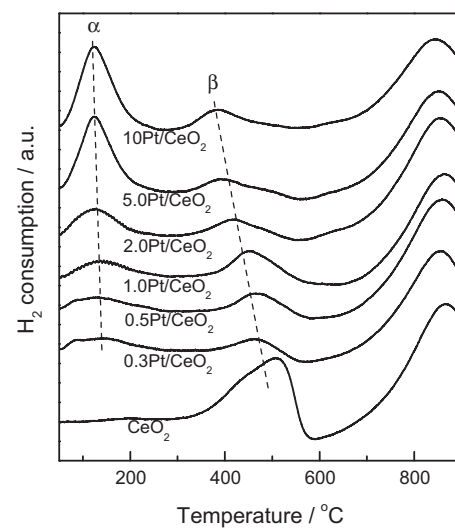
Catalysts	S_{BET} ($\text{m}^2 \text{ g}^{-1}$)	Pt content (wt.%)	Pt dispersion	Pt particle size (nm)	CeO ₂ crystallite size (nm)	Lattice parameter (nm)
CeO ₂	31	–	–	–	11.2	0.54109
0.3Pt/CeO ₂	35	0.33	0.98	1.2	11.2	0.54104
0.5Pt/CeO ₂	38	0.50	0.71	1.6	11.0	0.54103
1.0Pt/CeO ₂	39	1.13	0.52	2.2	11.1	0.54096
2.0Pt/CeO ₂	44	2.00	0.46	2.5	11.0	0.54099
5.0Pt/CeO ₂	46	4.73	0.23	5.0	11.1	0.54097
10Pt/CeO ₂	48	9.71	0.15	7.5	11.3	0.54091

d-spacing measurements. Also, the observed Pt particle sizes of the catalysts are about 1–8 nm (depending on the Pt content in the catalyst), which are well consistent with the CO chemisorption results (Table 1).

Chemical states of the Pt species in the Pt/CeO₂ catalysts were analyzed by XPS and representative results of the 0.3Pt/CeO₂, 2.0Pt/CeO₂ and 10Pt/CeO₂ catalysts are shown in Fig. 2. Peak intensities of the samples significantly increase with increasing Pt content in the catalyst (Note that the scales of the intensities are different for the catalysts). The Pt4f_{5/2} peaks of all these catalysts could be deconvoluted to two peaks at 71.2–71.5 and 72.1–72.7 eV, which could be assigned to Pt⁰ and Pt²⁺, respectively [26,27]. Note that the binding energy of the Pt4f_{5/2} peak in the 0.3Pt/CeO₂ (71.5 eV) is slightly higher than that in the 10Pt/CeO₂ (71.2 eV), indicating a stronger interaction between Pt and CeO₂ in the former sample. Even though the samples were pre-reduced before XPS measurement, oxidized Pt species are still present in the samples, which could be due to the strong interaction between Pt and CeO₂ (e.g. the formation of Pt–Ce–O solid solution). Compositions of different Pt species were also evaluated. It is found that the catalysts contain mainly metallic Pt (content of Pt⁰> 59%). The contents of Pt⁰ and Pt²⁺ species in these catalysts are essentially the same, and the slight deviations of the Pt⁰/Pt²⁺ ratios are within the analysis error because the peak intensities of the low Pt-content sample (e.g. 0.3Pt/CeO₂) are quite low. Also, the XPS spectra of O1s and Ce3d of the catalysts were also analyzed, as shown in Figs. S2 and S3, respectively (Figs. S2 and S3 in Supplementary Information). For the O1s spectra, one strong peak at 529.3 eV and one weak peak at 531.0 eV are observed, which could be assigned to lattice oxygen (O_{latt}) and surface adsorbed oxygen (O_{ads}), respectively

[28]. Meanwhile, the O_{latt}/O_{ads} ratios are 0.86/0.14, 0.82/0.18 and 0.81/0.19 for the 0.3Pt/CeO₂, 2.0Pt/CeO₂ and 10Pt/CeO₂ catalysts, respectively. The O_{latt}/O_{ads} ratio suggests that the concentration of the surface oxygen species (O_{ads}) on the 10Pt/CeO₂ is slightly higher compared to that on the 0.3Pt/CeO₂. For the Ce3d spectra (Fig. S3), the peaks could be deconvoluted to several components at 881.1 (v₀), 882.8 (v), 885.5 (v'), 888.8 (v''), 898.2 (v'''), 899.0 (u₀), 901.2 (u), 903.9 (u'), 907.0 (u'') and 916.5 eV (u'''). The v₀, v', u₀ and u' components could be assigned to Ce³⁺, while the v, v', v'', u, u'' and u''' components could be assigned to Ce⁴⁺ [29]. The co-existence of Ce³⁺ and Ce⁴⁺ species is due to the defects on the CeO₂ surface (e.g. oxygen vacancies). Also, the Ce³⁺/Ce⁴⁺ ratios of these catalysts are quite similar, which are 0.28/0.72, 0.34/0.66 and 0.31/0.69 for the 0.3Pt/CeO₂, 2.0Pt/CeO₂ and 10Pt/CeO₂ catalysts, respectively.

Reduction properties of the Pt/CeO₂ catalysts were measured by H₂-TPR and the profiles are shown in Fig. 3. For the pure CeO₂ support, only an intense peak in range of 320–580 °C is observed, which could be attributed to the reduction of surface Ce⁴⁺. For the supported Pt/CeO₂ catalysts, a low-temperature reduction peak centered at about 150 °C (α peak) and a high-temperature reduction peak in the range of 360–600 °C (β peak) are observed. The peak at 150 °C could be assigned to the reduction of PtO_x [30]. Note that the α peak also contains the contribution of the reduction of Ce⁴⁺ ions adjacent to Pt species due to a spillover effect, because the actual amounts of H₂ consumption for the 0.3Pt/CeO₂, 0.5Pt/CeO₂, 1.0Pt/CeO₂, 2.0Pt/CeO₂, 5.0Pt/CeO₂ and 10Pt/CeO₂ are 0.08, 0.083, 0.095, 0.137, 0.320 and 0.356 mmol_{H₂} g_{cat}⁻¹ respectively, which are significantly higher than the nominal values (0.018, 0.026, 0.058, 0.102, 0.256 and 0.500 mmol_{H₂} g_{cat}⁻¹ for 0.3Pt/CeO₂, 0.5Pt/CeO₂, 1.0Pt/CeO₂, 2.0Pt/CeO₂, 5.0Pt/CeO₂ and 10Pt/CeO₂, respectively, assuming that the Pt species in the catalyst are Pt²⁺). The β peak could be attributed to the reduction of surface CeO₂ caused by the spillover effect, which is confirmed by the fact that

**Fig. 2.** XPS results of (a) 0.3Pt/CeO₂, (b) 2.0Pt/CeO₂ and (c) 10Pt/CeO₂ catalysts.**Fig. 3.** H₂-TPR profiles of Pt/CeO₂ catalysts.

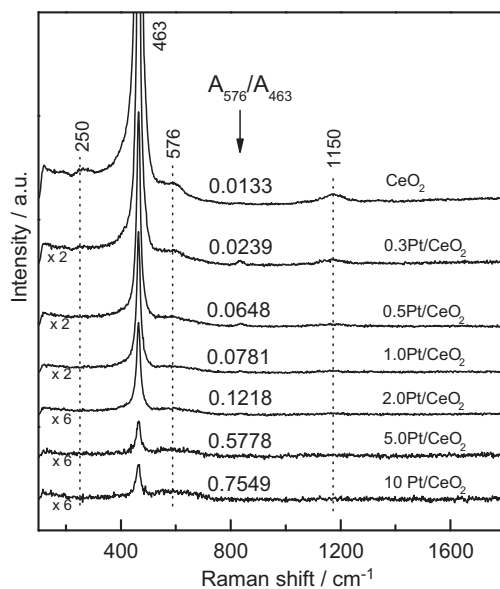


Fig. 4. Raman spectra of Pt/ CeO_2 catalysts.

this peak gradually shifts to lower temperature with increasing Pt content in the catalyst.

Fig. 4 shows the Raman spectra of the Pt/ CeO_2 catalysts, as well as the pure CeO_2 . All the catalysts have one distinct band at 463 cm^{-1} and three weak bands at 250 , 576 , 1150 cm^{-1} . The band at 463 cm^{-1} is due to the characteristic F_{2g} vibration mode of fluorite structure of CeO_2 [31] and the bands at 250 and 576 cm^{-1} are ascribed to oxygen vacancies [32], while the weak band at 1150 cm^{-1} is ascribed to primary A_{1g} asymmetry of CeO_2 [33]. The band at 576 cm^{-1} indicates the evolution of oxygen vacancies, which is generated from the formation of the Pt–Ce–O solid solution and the charge balance for the partial replacement of Ce^{4+} ions by Pt^{2+} ions. The peak areas of the bands at 463 and 576 cm^{-1} are calculated based on the results shown in Fig. 4, which are denoted as A_{463} and A_{576} , respectively. The ratio of A_{576}/A_{463} reflects the concentration of oxygen vacancies in these catalysts [34]. It can be seen that the A_{576}/A_{463} value increases with Pt content in the catalyst, implying increasing concentration of oxygen vacancies. This is in good agreement with the lattice parameter estimations (Table 1), as the lattice parameter of the Pt/ CeO_2 catalyst declines with increasing Pt content in the catalyst.

Fig. 5 presents the FTIR spectra of CO chemisorption on the Pt/ CeO_2 catalysts at 40°C . The pure CeO_2 support does not chemisorb CO. For the Pt-containing catalysts, bands at 2047 – 2071 cm^{-1} are clearly observed. This characteristic band could be assigned to linear chemisorption of CO on Pt^0 . The band intensity progressively increases with Pt content in the catalyst due to more exposed surface Pt atoms. Moreover, this band shifts to lower wavenumber with increasing Pt content. Such a red shift is not consistent with the findings on Pt/ Al_2O_3 catalysts with different Pt dispersions in which a blue-shift of the linear CO–Pt band with increasing Pt particles was observed. The authors attributed such trends to the changes in surface curvature and coordination with cluster size [9]. However, our finding is consistent with that reported on Pt/ CeO_2 catalysts [35]. Kalamaras et al. [35] found a CO–Pt band at about 2090 cm^{-1} on a $0.6\text{Pt}/\text{CeO}_2$ catalyst and a band at about 2082 cm^{-1} on a $2.0\text{Pt}/\text{CeO}_2$ but no explanation was given in this work [35]. Although a convincing interpretation on such red-shift could not be reached at the present stage, it is possible that the red-shift observed in the current work is related to several parameters such as surface coordination depending on the Pt particle size, the multiple chemical states of the Pt species (Pt^0 and

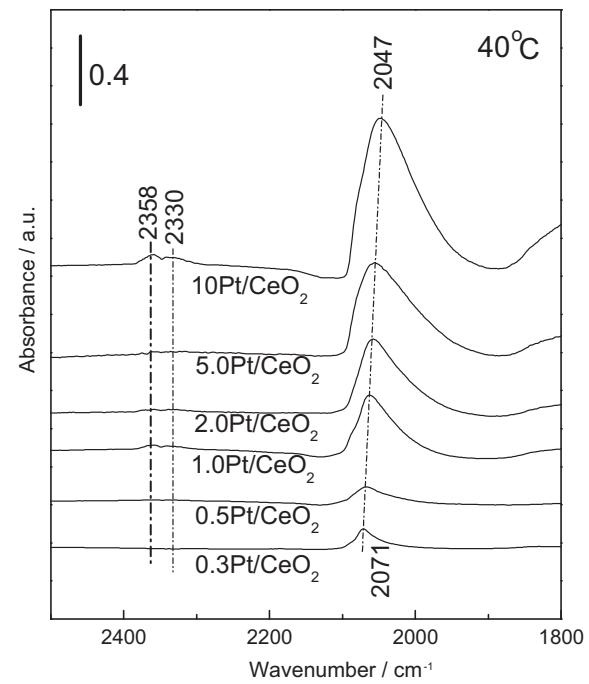


Fig. 5. FTIR spectra of CO chemisorption on various Pt/ CeO_2 catalysts at 40°C .

Pt^{2+}), and interaction between Pt– CeO_2 in the catalysts. In addition, note that the CO chemisorption on oxidized Pt species is not detected, as evidenced by the absence of bands at higher wavenumbers ($>2100\text{ cm}^{-1}$ for CO chemisorption on $\text{Pt}^{n+}(1 < n < 2)$ [36–38]). A possible explanation of the absence of the CO– Pt^{2+} band is that it could be related to the locations of these Pt^{2+} species in the catalyst. Most of the Pt^{2+} species are embedded in CeO_2 matrix due to the formation of Pt–Ce–O solid solution, which makes the CO molecules not accessible to these species. Similar findings were also reported in PdO/ CeO_2 [39] and CuO/ CeO_2 [23] catalysts. For example, Meng et al. [39] reported CO chemisorption on a PdO/ CeO_2 catalyst; however, there is no CO chemisorption on the catalyst when the surface Pd species were removed by a nitric acid treatment even though oxidized Pd species were detected in the catalyst (in form of Pd–Ce–O solid solution). Thus, in the current case we believe that the CO chemisorption on the Pt/ CeO_2 catalysts mainly takes place on the surface metallic Pt species (as the catalysts were pre-reduced in H_2) but the oxidized Pt species are not accessible for the CO molecules.

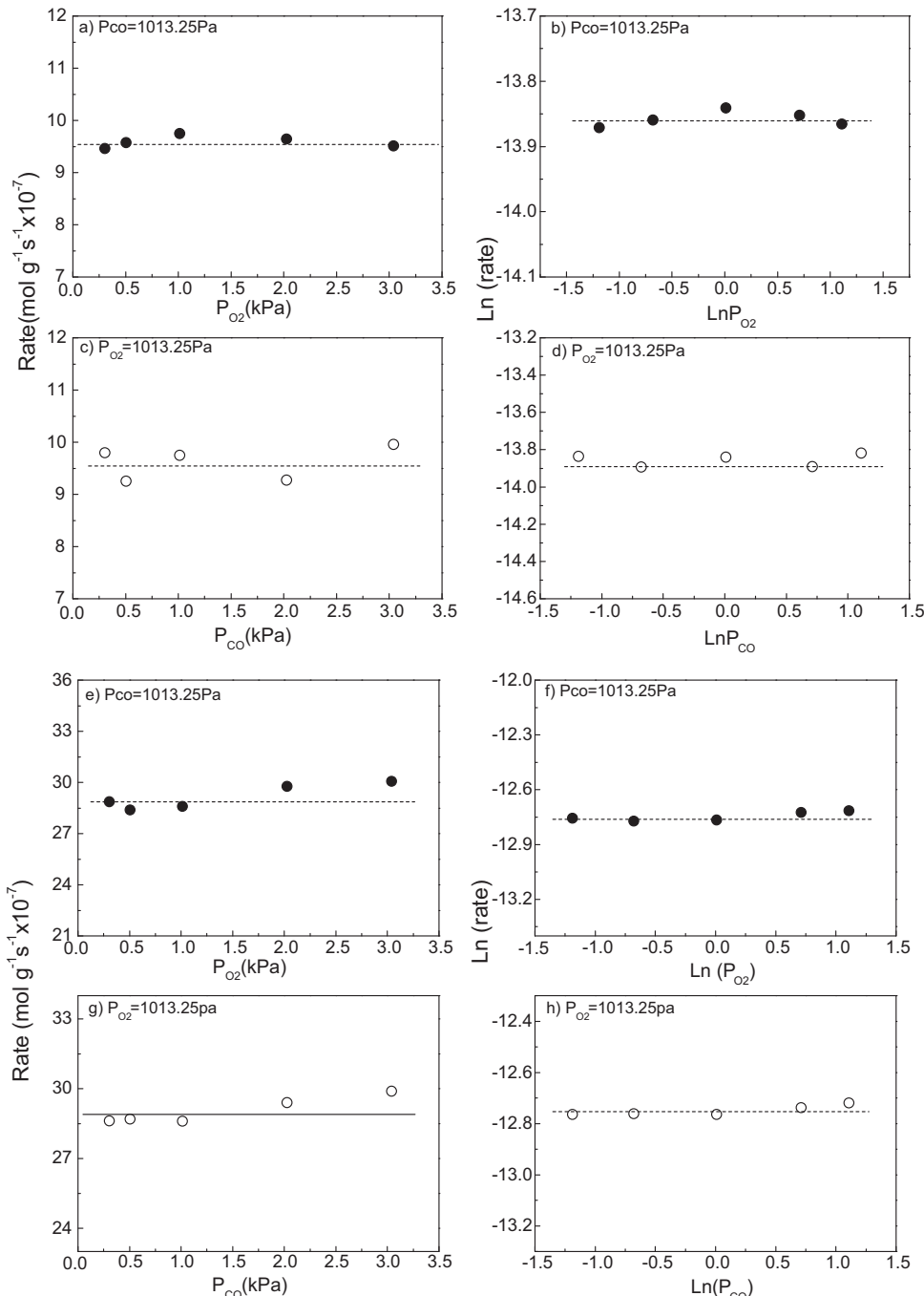
The characterization results suggest that by changing the Pt loadings, catalysts with Pt sizes ranging from 1 to 8 nm were prepared. Formation of Pt–Ce–O solid solution is evidenced by the XRD and Raman spectroscopy results. The oxidation states of these catalysts were also analyzed by XPS technique, which suggests the presence of both metallic and oxidized Pt species in the catalysts.

3.2. Kinetic study of CO oxidation over $0.5\text{Pt}/\text{CeO}_2$ and $2.0\text{Pt}/\text{CeO}_2$ catalysts

Kinetic study of CO oxidation was performed on the $0.5\text{Pt}/\text{CeO}_2$ and $2.0\text{Pt}/\text{CeO}_2$ catalysts. Absence of mass and heat transfer limitation was verified by checking the Weisz–Prater criterion and Mears' criterion. The reaction was carried out at differential mode with CO conversions typically less than 15% . By changing partial pressures of CO and O_2 , a series of CO conversions were obtained and consequently reaction rates in unit of $\text{mol}_{\text{CO}} \text{ g}_{\text{cat}}^{-1} \text{ s}^{-1}$ were obtained, as summarized in Table 2. It is found that for each catalyst the reaction rate remains almost constant, despite of various concentrations of

Table 2Summary of kinetic results for CO oxidation over Pt/CeO₂ catalysts at 40 °C.

Partial pressure (kPa)		CO conv. (%)		Reaction rate ($\times 10^{-7}$ mol g ⁻¹ s ⁻¹)		Power rate expression
CO	O ₂	0.5Pt/CeO ₂ (50 mg)	2.0Pt/CeO ₂ (30 mg)	0.5Pt/CeO ₂ (50 mg)	2.0Pt/CeO ₂ (30 mg)	
1.0133	0.3040	5.3	9.7	9.46	28.87	0.5Pt/CeO ₂
1.0133	0.5066	5.4	9.5	9.57	28.30	$r = 8.04 \times 10^{-7} P_{CO}^0 P_{O_2}^0$
1.0133	1.0133	5.5	9.6	9.75	28.61	$E_a = 45.6 \text{ kJ mol}^{-1}$
1.0133	2.0265	5.4	10.0	9.64	29.76	
1.0133	3.0398	5.3	10.1	9.51	30.06	2.0Pt/CeO ₂
0.3040	1.0133	18.3	29.8	9.80	26.61	$r = 2.72 \times 10^{-6}$
0.5066	1.0133	10.4	19.3	9.25	28.70	$P_{CO}^{0.01} P_{O_2}^{0.03}$
2.0265	1.0133	2.6	4.9	9.27	29.38	$E_a = 51.0 \text{ kJ mol}^{-1}$
3.0398	1.0133	1.9	3.3	9.96	29.89	

**Fig. 6.** Kinetic results of CO oxidation over (a)–(d) 0.5 Pt/CeO₂ and (e)–(h) 2.0 Pt/CeO₂ at 40 °C.

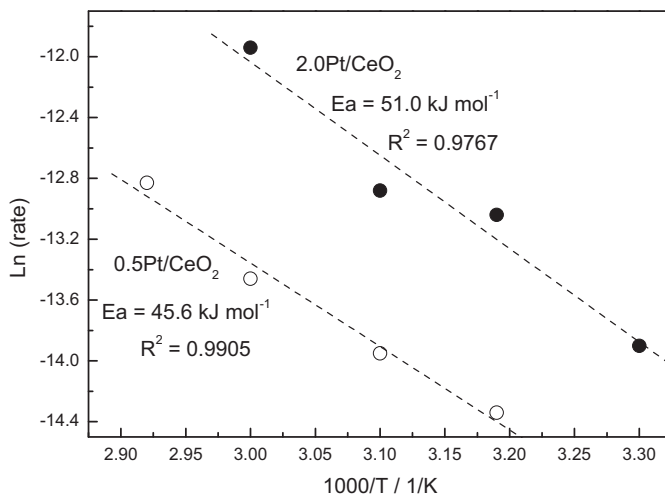


Fig. 7. Arrhenius plots of CO oxidation over (a) 0.5Pt/CeO₂ and (b) 2.0 Pt/CeO₂ catalysts.

CO and O₂ in the feedstock. Also the 2.0Pt/CeO₂ is more active than the 0.5Pt/CeO₂. The dependences of partial pressures of CO and O₂ on the reaction rate are demonstrated in Fig. 6. After taking logarithm of these values, the reaction order of CO and O₂ could be calculated. Thus, the power rate expression for the 0.5Pt/CeO₂ is $r = 8.04 \times 10^{-7} P_{CO}^0 P_{O_2}^0$, while the expression for the 2.0Pt/CeO₂ is $r = 2.72 \times 10^{-6} P_{CO}^{0.01} P_{O_2}^{0.03}$. The expressions clearly indicate that the reaction rate is essentially independent on the partial pressures of CO and O₂, which is in line with the findings in a previous work [16].

The apparent activation energies for these catalysts were calculated via Arrhenius plots shown in Fig. 7. The values are 45.6 kJ mol⁻¹ for the 0.5Pt/CeO₂ and 51.0 kJ mol⁻¹ for the 2.0Pt/CeO₂. These values are higher than those obtained over Pt/SiO₂ catalysts (13–22 kJ mol⁻¹ [12]), but are lower than those obtained on Pt/Al₂O₃ catalysts (65–90 kJ mol⁻¹ [9]). But they are comparable to those obtained on the Pt/TiO₂ catalysts (41.5 kJ mol⁻¹) [13] and those on similar Pt/CeO₂ catalysts (42–63 kJ mol⁻¹) [16]. Moreover, similar activation energies (45.6 vs 51.0 kJ mol⁻¹) imply that the reaction pathways might be the same on these two catalysts.

Based on the rate expression, elementary steps of CO oxidation over the Pt/CeO₂ could be derived. Indeed, reaction pathways over Pt catalysts for CO oxidation have been proposed in literature. For example, in some works, classic Langmuir–Hinshelwood models involving competitive adsorption and reaction of CO and O₂ on Pt surface in Pt/Al₂O₃ catalysts were proposed [9,40], as well as non-competitive adsorption of CO and O₂ on Pt surface atoms in Pt/SiO₂ catalysts [12]. In the case of competitive adsorption and reaction of CO and O₂ on Pt surface, rate expressions $r = (k_3 K_1 K_2 [O_2][CO]) / ((1 + K_1[CO])^2)$ [9] or $r = (k_2 [O_2]) / ((1 + K_1[CO]))$ [40] were deduced, which resulted in a negative reaction order on CO partial pressure (−1 at near saturation of CO coverage) and a reaction order of 1 on O₂ partial pressure. These expressions are not consistent with the kinetic results in the current work and thus could be ruled out. In the case of non-competitive adsorption of CO and O₂ on Pt surface atoms, a rate expression $r = (k_3 K_1 K_2^{1/2} [CO][O_2]^{1/2}) / ((1 + K_1[CO])(1 + K_2^{1/2}[O_2]^{1/2}))$ was obtained [12], which could be further simplified to $r = k_3 K_2^{1/2} [O_2]^{1/2}$ at near saturation CO coverage and low O coverage ($K_1[CO] \gg 1$ and $K_2^{1/2}[O_2]^{1/2} \ll 1$). This expression could also be excluded as it is not consistent with the kinetic results in the current work.

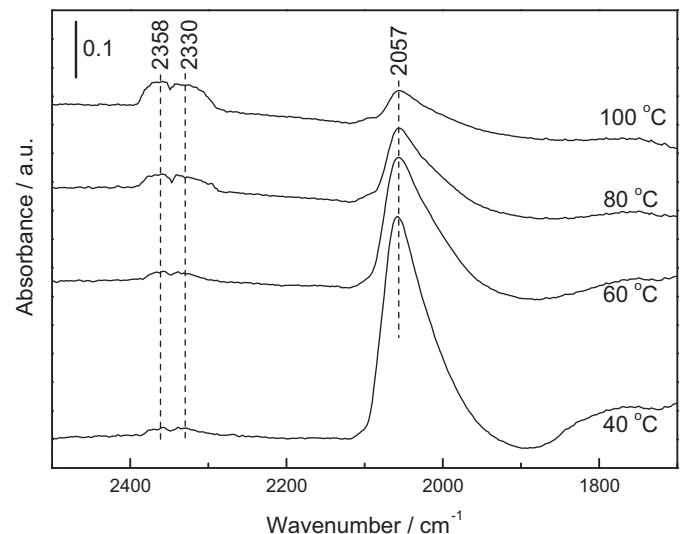
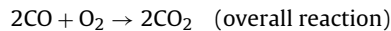
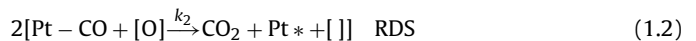


Fig. 8. FTIR spectra of CO chemisorption over 2.0Pt/CeO₂ catalyst at elevated temperatures.

CeO₂ is a typical reducible oxide and the lattice oxygen in CeO₂ often participate in CO oxidation, which leads to a zero dependence of O₂ partial pressure in the rate expressions [23,41,42]. The involvement of the lattice oxygen in the reaction is also confirmed by in situ FTIR results of CO chemisorption over the 2.0Pt/CeO₂, as shown in Fig. 8. It is found that with increasing temperature from 40 to 100 °C, the intensity of the band at 2057 cm⁻¹ assigning to chemisorbed CO on Pt declines significantly, due to the desorption of CO from the catalyst surface or the consumption of CO. Meanwhile, broad bands in range of 2300–2400 cm⁻¹ assigning to gas phase CO₂ progressively increase in intensity, implying the formation of CO₂. Note that there is no O₂ in the feed gas, the formation of CO₂ is most likely due to the reaction between CO and lattice oxygen or surface oxygen species.

Based on these facts, elementary steps of CO oxidation over the Pt/CeO₂ catalysts are proposed as follows, which follows a Mars van-Krevelen reaction model:



where [O] refers to lattice oxygen and [] refers to oxygen vacancy.

The basic assumptions of CO oxidation over Pt/CeO₂ are as follows:

- 1 Chemisorption of CO on surface Pt atoms to form Pt-CO species (Eq. (1.1)).
- 2 Migration of the Pt-CO species to the Pt-CeO₂ interface and reacting with lattice oxygen provided by CeO₂, which is considered as the RDS (Eq. (1.2)).
- 3 Refilling of oxygen vacancies by gas-phase O₂ (Eq. (1.3)).

With these elementary steps ((1.1)–(1.3)), the reaction rate expression is:

$$r = \frac{k_2 K_1 [CO][O]}{(1 + K_1[CO])}$$

The CO chemisorption on Pt surface atoms is verified by the FTIR results (Fig. 4), and the involvement of lattice oxygen in

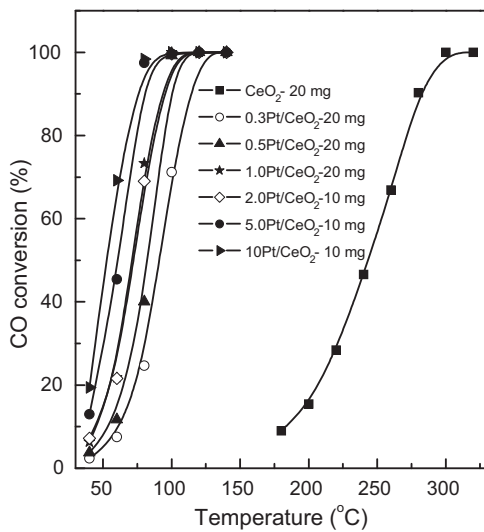


Fig. 9. Light-off curves of CO oxidation over Pt/CeO₂ catalysts.

the reaction is also verified by the FTIR results (Fig. 8). If CO chemisorption on Pt is near saturation ($K_2[\text{CO}] \gg 1$), and note that the concentration of lattice oxygen in the CeO₂ support is a constant, the rate expression could be simplified to $r = k_{\text{app}}[\text{CO}]^0[\text{O}_2]^0$ ($k_{\text{app}} = k_2$). This rate expression fits well with the kinetic results. Thus, this reaction model demonstrates an interfacial reaction between the chemisorbed CO on Pt atoms and lattice oxygen in the CeO₂ support, with the interfacial Pt–O–Ce ensembles being the active sites. This model is in consistent with that reported by Cargnello et al. [16], in which they reported dependences of −0.01 for CO and 0.1 for O₂ over Pt/CeO₂ catalysts for CO oxidation. The authors concluded that such dependences were a result of reaction between CO adsorbed on the Pt and O₂ provided by the CeO₂.

3.3. Catalytic testing and effect of Pt particle size on CO oxidation

CO oxidation over various Pt/CeO₂ catalysts with different Pt loadings was also tested and the results are shown in Fig. 9. Note that in order to obtain CO conversions at low levels (<20%) especially at low reaction temperatures (e.g. 40 °C), different weights of some catalysts were employed. Also, detailed results at the reaction temperature of 40 °C are listed in Table 3. Due to the different Pt contents in the catalysts, the catalytic performances of the catalysts were normalized to specific reaction rate in unit of mmol_{CO} g_{Pt}⁻¹ h⁻¹. As shown in Table 3, it is found that the rate declines with Pt content in the catalyst, from 551.6 mmol_{CO} g_{Pt}⁻¹ h⁻¹ on the 0.3Pt/CeO₂ to 223.6 mmol_{CO} g_{Pt}⁻¹ h⁻¹ on the 10Pt/CeO₂. Concerning more intrinsic reactivities of these catalysts, turnover frequencies (TOFs) based on two different models were also calculated (Table 3). The TOF_a values reflecting all surface Pt atoms show that the values increase with increasing Pt contents in the catalysts, ranging

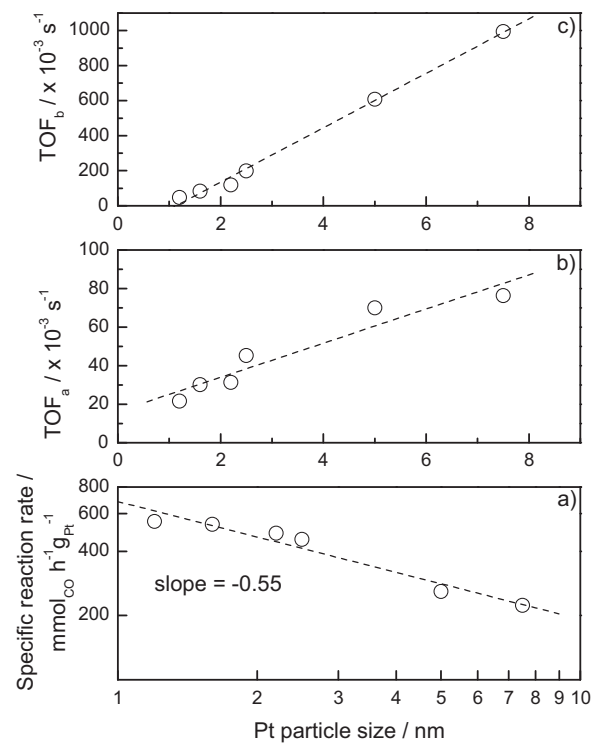


Fig. 10. Relationship between specific reaction rate, TOF_a and TOF_b and Pt particle size at 40 °C.

from $21.3 \times 10^{-3} \text{ s}^{-1}$ on the 0.3Pt/CeO₂ to $76.3 \times 10^{-3} \text{ s}^{-1}$ on the 10Pt/CeO₂. As for the TOF_b values reflecting the periphery Pt atoms at the Pt–CeO₂ interface, it is also found that the values increase with Pt contents, ranging from $46.9 \times 10^{-3} \text{ s}^{-1}$ on the 0.3Pt/CeO₂ to $994.0 \times 10^{-3} \text{ s}^{-1}$ on the 10Pt/CeO₂.

To better demonstrate the relationship between reactivity and Pt particle size, specific reaction rate, TOF_a and TOF_b versus Pt particle size in the catalysts were plotted, as shown in Fig. 10 based on the data in Table 3. In Fig. 10a, it is found that the specific reaction rate is proportional to $d^{-0.55}$ (d is Pt particle size). In a previous work by Cargnello et al. [16], they reported a Pt particle size dependence of −2 on Pt/CeO₂ catalysts for CO oxidation and the authors concluded that such a dependence (−2) indicated the interfacial reaction. In the current work, the dependence (−0.55) is much higher than that reported in literature (−2), suggesting more complicated involvement of Pt and the CeO₂ support in the reaction. As for the TOF_a, Fig. 10b shows that the TOF_a values increase almost linearly with Pt particle size. Such a trend is obviously not in consistent with the previous findings on Pt/Al₂O₃ [9], Pt/TiO₂ [13] and even on Pt/CeO₂ [16], but is in agreement with the findings on Pt/SiO₂ [12]. On Pt/SiO₂ catalysts, Gracia et al. [12] suggested that the changes in the intrinsic activity (TOF) was due to the altering of the fractions of Pt atoms at low coordination sites (i.e. corners and edges) and the atoms on planar faces, and they believed that the Pt atoms on planar faces were much more active than those on corners and edges. Even though the changing trends in Pt/SiO₂ catalysts and Pt/CeO₂ catalysts in the current work are the same, obvious differences exist in these systems. For the Pt/SiO₂ catalysts, chemisorption of CO and O₂ occur on Pt surface, which may result in different activation barriers on different sites. However, for the Pt/CeO₂ catalysts, CO oxidation takes place the Pt–CeO₂ interface and the interfacial Pt atoms are the active sites for this reaction, as confirmed by the kinetics in the current work, as well as in previous work [16], and thus the interfacial atoms are apparently more active than the surface atoms [16]. Therefore, the same changing trends

Table 3

Summary of catalytic results for CO oxidation over Pt/CeO₂ catalysts at 40 °C.

Catalyst	m_{cat} (mg)	CO conv. (%)	Specific reaction rate (mmol _{CO} g _{Pt} ⁻¹ h ⁻¹)	TOF ($\times 10^{-3} \text{ s}^{-1}$)	
				TOF _a	TOF _b
0.3Pt/CeO ₂	20	2.4	551.6	21.6	46.9
0.5Pt/CeO ₂	20	3.7	535.0	30.1	83.8
1.0Pt/CeO ₂	20	6.3	486.9	31.4	119.3
2.0Pt/CeO ₂	10	7.2	455.3	45.2	199.0
5.0Pt/CeO ₂	10	13.0	258.9	69.9	607.7
10Pt/CeO ₂	10	19.4	223.6	76.3	994.0

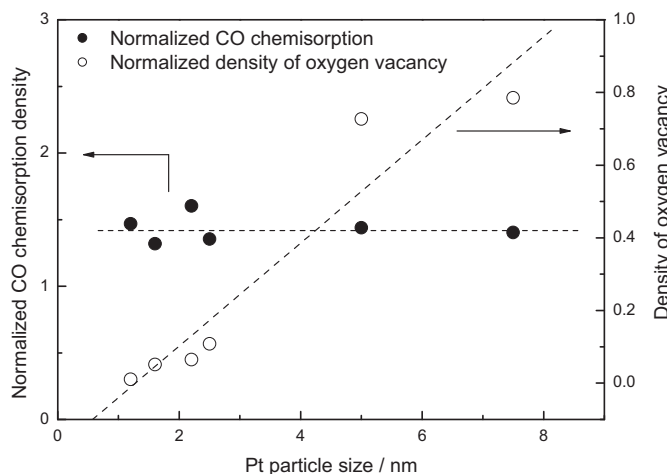


Fig. 11. Relationship between CO chemisorption and oxygen vacancy and Pt particle size.

of TOFs in the current work and in the Pt/SiO₂ system seem more like a coincidence and they do not share similar interpretations.

More interestingly, if an interfacial reaction is proposed as in the current work, TOFs calculated based on interfacial Pt atoms seem more reasonable because these atoms are the active sites for CO oxidation. As shown in Fig. 10c, it is found that the TOF_b values also increase with increasing Pt particle size. Note that the calculation of the TOF_b may contain considerable error because of the inhomogeneous Pt particle distributions in the catalysts, but the largely deviated values (46.9×10^{-3} – $994.0 \times 10^{-3} \text{ s}^{-1}$) certainly suggest that CO oxidation over Pt/CeO₂ catalysts is structure-sensitive; however, it is not consistent with the reported findings that the activities of the interfacial atoms were independent on the metal particle size of Au [17,18] or Pt [13,16]. Thus, the discrepancy certainly deserves a discussion. According to the reaction pathways on the Pt/CeO₂ (Eqs. (1.1)–(1.3)), the rate is determined by the reaction between the chemisorbed CO and the lattice oxygen ($r = k_2[\text{Pt}-\text{CO}][\text{O}]$ derived from Eq. (1.2)). As the concentration of Pt-CO is a constant at near saturation condition, as well as that of the lattice oxygen ($[\text{O}]$), then the rate is practically dependent on the rate constant k_2 . The rate constant k_2 is related to the mobility of lattice oxygen in the CeO₂ support, namely, easier mobility of lattice oxygen would result in a larger k_2 value. It is well known that the mobility of lattice oxygen in CeO₂ oxide could be significantly promoted in the presence of oxygen vacancy [43,44]. In the current work, in order to confirm the roles of CO chemisorption and oxygen vacancy, normalized FTIR band intensity at 2047–2071 cm⁻¹ (in Fig. 5) and concentrations of oxygen vacancy in different samples (A₅₇₆/A₄₆₃ in Fig. 4) are correlated to Pt particle sizes in the catalysts, as shown in Fig. 11. The normalized CO chemisorption was based on the peak area of the band divided by Pt content and dispersion in the catalyst. It is clear that the CO density on surface Pt atoms is almost constant, which is in expectation because the CO are saturated on Pt surface. As for the oxygen vacancy, it increases linearly with Pt content in the catalyst. Although the correlation could not be taken as a quantitative analysis, such a trend explains well the higher TOF values on the large Pt particles. The migration of lattice oxygen in the catalyst with large Pt particles is more pronounced than that in the catalyst with small Pt particles as the former catalyst contains much more oxygen vacancies, which would lead to a larger k_2 (or k_{app}). This point is clearly evidenced by the comparison of the rate constants obtained on the 0.5Pt/CeO₂ and 2.0Pt/CeO₂ catalysts, which are 8.04×10^{-7} and 2.72×10^{-6} , respectively (Table 2). Also, the findings in the Pt/CeO₂ catalysts are in good agreement with our previous work on CO oxidation over Cu-Ce-O solid solu-

tions [23]. It was found that the activity was proportional to the concentration of oxygen vacancy in the sample, suggesting a pivotal role of oxygen vacancy in the CO oxidation. Similar role of the presence of oxygen vacancies in CO oxidation was also observed on PdO-CeO₂ catalysts [39], which was also evidenced by theoretical calculation [45]. Another noteworthy point is the contributions of Pt⁰ and Pt²⁺ species in the reactivity in CO oxidation. Although debates still exist [46,47], a recent work by Gao et al. [48] concluded that in Pt/CeO₂ catalyst, Pt⁰ species were more active than the Pt²⁺ species for CO oxidation. In the current work, it is likely that most of the oxidized Pt species (Pt²⁺) are located in the CeO₂ matrix via the formation of Pt-Ce-O solid solution, thus their contributions to the reactivity could be very limited. Therefore, although a quantitative analysis is difficult at present, the Pt⁰ species in the Pt/CeO₂ may play dominant role in the CO oxidation.

Besides, compared with the current work, the constant TOF values based on interfacial Pt atoms (refers to TOF_b in the current work) of Pt/CeO₂ catalysts reported by Cagnello et al. [16] might be due to the different natures of these catalysts. In their work, the Pt/CeO₂ catalyst were prepared by deposition of as-synthesized Pt nanoparticles on the CeO₂ support and followed by low temperature calcination at 300 °C. Such a procedure may not result in incorporation of Pt cations in the CeO₂ lattice and thus make the Pt-CeO₂ interface unchanged in spite of different Pt loadings, which accounts for the constant TOFs on these catalysts. But in the current work, the Pt/CeO₂ catalysts were prepared by the impregnation of Pt²⁺ cations (with Pt(NO₃)₂ as the precursor) on the CeO₂ support, which resulted in penetration of Pt cations in the CeO₂ lattice (as confirmed by XRD and Raman results) and thus make the Pt-CeO₂ interface differ in these catalysts.

4. Conclusion

This work demonstrates CO oxidation over a series of Pt/CeO₂ catalysts. The kinetic study reveals that the reaction rate is independent of the partial pressures of CO and O₂, indicating a Mars van-Krevelen type reaction on these catalysts, with CO chemisorbed on surface Pt atoms and reacting with lattice oxygen provided by CeO₂ at the Pt-CeO₂ interface. Moreover, the effect of Pt particle size on the reaction is also investigated and it is found that the formation of Pt-Ce-O solid solution plays an important role in accelerating the reaction.

Acknowledgment

This work is financially supported by National Natural Science Foundation of China (grant nos. 21173195 and 21203167).

Appendix A. Supplementary data

Supplementary data associated with this article can be found, in the online version, at doi:10.1016/j.apsusc.2014.06.196.

References

- [1] D.R. Schryer, B.T. Upchurch, B.D. Sidney, K.G. Brown, G.B. Hoflund, R.K. Herz, *J. Catal.* 130 (1991) 314–317.
- [2] Y.Z. Yuan, A.P. Kozlova, K. Asakura, H.L. Wan, K. Tsai, Y. Iwasawa, *J. Catal.* 170 (1997) 191–199.
- [3] M. Haruta, T. Kobayashi, H. Sano, N. Yamada, *Chem. Lett.* 16 (1987) 405–408.
- [4] M. Haruta, S. Tsubota, T. Kobayashi, H. Kageyama, M.J. Genet, B. Delmon, *J. Catal.* 144 (1993) 175–192.
- [5] M. Fernández-García, A. Martínez-Arias, L.N. Salamanca, J.M. Coronado, J.A. Anderson, J.C. Conesa, J. Soria, *J. Catal.* 187 (1999) 474–485.
- [6] S.M. McClure, D.W. Goodman, *Chem. Phys. Lett.* 469 (2009) 1–13.
- [7] D.R. Schryer, B.T. Upchurch, J.D. Van Norman, K.G. Brown, J. Schryer, *J. Catal.* 122 (1990) 193–197.
- [8] M. Che, C.O. Bennett, *Adv. Catal.* 36 (1989) 55–172.

- [9] A.D. Allian, K. Takanabe, K.L. Fajdala, X. Hao, T.J. Truex, J. Cai, C. Buda, M. Neurack, E. Iglesia, *J. Am. Chem. Soc.* 133 (2011) 4498–4517.
- [10] N.W. Cant, *J. Catal.* 62 (1980) 173–175.
- [11] D.R. Rainer, M. Koranne, S.M. Vesecky, D.W. Goodman, *J. Phys. Chem. B* 101 (1997) 10769–10774.
- [12] F.J. Gracia, J.T. Miller, A.J. Krof, E.E. Wolf, *J. Catal.* 209 (2002) 341–354.
- [13] N. Li, Q.Y. Chen, L.F. Luo, W.X. Huang, M.F. Luo, G.S. Hu, J.Q. Lu, *Appl. Catal. B: Environ.* 142–143 (2013) 523–532.
- [14] S. Salomons, R.E. Hayes, M. Votsmeier, *Appl. Catal. B: Environ.* 70 (2007) 305–313.
- [15] R.H. Venderbosch, W. Prins, W.P.M. Van Swaaij, *Chem. Eng. Sci.* 53 (1998) 3355–3366.
- [16] M. Cargnello, V. Doan-Nguyen, T.R. Gordon, R.E. Diaz, E.A. Stach, R.J. Gorte, P. Fornasiero, C.B. Murray, *Science* 341 (2013) 771–773.
- [17] S.H. Overbury, V. Schwartz, D.R. Mullins, W. Yan, S. Dai, *J. Catal.* 241 (2006) 56–65.
- [18] T. Fujitani, I. Nakamura, *Angew. Chem. Int. Ed.* 50 (2011) 10144–10147.
- [19] Y. Maeda, Y. Iizuka, M. Kohyama, *J. Am. Chem. Soc.* 135 (2013) 906–909.
- [20] A. Martínez-Arias, A.B. Hungría, M. Fernández-García, J.C. Conesa, G. Munuera, *J. Phys. Chem. B* 108 (2004) 17983–17991.
- [21] J.Q. Lu, C.X. Sun, N. Li, A.P. Jia, M.F. Luo, *Appl. Surf. Sci.* 287 (2013) 124–134.
- [22] K. Qian, Z. Qian, Q. Hua, Z. Jiang, W. Huang, *Appl. Surf. Sci.* 273 (2013) 357–363.
- [23] A.P. Jia, G.S. Hu, L. Meng, Y.L. Xie, J.Q. Lu, M.F. Luo, *J. Catal.* 289 (2012) 199–209.
- [24] H.S. Fogler, *Elements of Chemical Reaction Engineering*, 4th ed., Pearson Education Inc., 2006, pp. 839.
- [25] M. Shacham, M.B. Cutlip, M. Elly, Polymath, Copyright, 2006 <http://www.polymath-software.com>
- [26] J. Silvestre-Albero, J.C. Serrano-Ruiz, A. Sepúlveda-Escribano, F. Rodríguez-Reinoso, *Appl. Catal. A: Gen.* 292 (2005) 244–251.
- [27] A.M. Ruppert, T. Paryjczak, *Appl. Catal. A: Gen.* 320 (2007) 80–90.
- [28] A. Machocki, T. Ioannides, B. Stasinska, W. Gac, G. Avgouropoulos, D. Delimaris, W. Grzegorczyk, S. Pasieczna, *J. Catal.* 227 (2004) 282–296.
- [29] C. Anandan, P. Bera, *Appl. Surf. Sci.* 283 (2013) 297–303.
- [30] P. Reyes, G. Pecchi, M. Morales, J.L.G. Fierro, *Appl. Catal. A: Gen.* 163 (1997) 145–152.
- [31] W.H. Weber, K.C. Hass, J.R. McBride, *Phys. Rev. B* 48 (1993) 178–185.
- [32] J.R. McBride, K.C. Hass, B.D. Poindexter, W.H. Weber, *J. Appl. Phys.* 76 (1994) 2435–2441.
- [33] S. Velu, K. Suzuki, T. Osaki, *Catal. Lett.* 62 (1999) 159–167.
- [34] Z.Y. Pu, J.Q. Lu, M.F. Luo, Y.L. Xie, *J. Phys. Chem. C* 111 (2007) 18695–18702.
- [35] C.M. Kalamaras, S. Americanou, A.M. Efstathiou, *J. Catal.* 279 (2011) 287–300.
- [36] O.S. Alexeev, S.Y. Chin, M.H. Engelhard, L. Ortiz-Soto, M.D. Amiridis, *J. Phys. Chem. B* 109 (2005) 23430–23443.
- [37] P. Panagiotopoulou, A. Christodoulakis, D.I. Kondarides, S. Boghosian, *J. Catal.* 240 (2006) 114–125.
- [38] P.A. Carlsson, L. Österlund, P. Thormählen, A. Palmqvist, E. Fridell, J. Jansson, M. Skoglundh, *J. Catal.* 226 (2004) 422–434.
- [39] L. Meng, A.P. Jia, J.Q. Lu, L.F. Luo, W.X. Huang, M.F. Luo, *J. Phys. Chem. C* 115 (2011) 19789–19796.
- [40] G. Djéga-Mariadassou, M. Boudart, *J. Catal.* 216 (2003) 89–97.
- [41] W. Liu, M. Flytzani-Stephanopoulos, *J. Catal.* 153 (1995) 317–332.
- [42] M. Moreno, G.T. Baronti, M.A. Laborde, F.J. Marino, *Int. J. Hydrogen Energy* 33 (2008) 3538–3542.
- [43] G. Sedmak, S. Hočvar, J. Levec, *J. Catal.* 222 (2004) 87–99.
- [44] G. Sedmak, S. Hočvar, J. Levec, *J. Catal.* 213 (2003) 135–150.
- [45] W.G. Reimers, M.A. Baltanas, M.M. Branda, *Appl. Surf. Sci.* 274 (2013) 1–6.
- [46] C.S. Polster, R. Zhang, M.T. Cyb, J.T. Miller, C.D. Baertsch, *J. Catal.* 273 (2010) 50–58.
- [47] Y. Zhai, D. Pierre, R. Si, W. Deng, P. Ferrin, A.U. Nilekar, G. Peng, J.A. Herron, D.C. Bell, H. Saltsburg, M. Mavrikakis, M. Flytzani-Stephanopoulos, *Science* 329 (2010) 1633–1636.
- [48] Y. Gao, W. Wang, S. Chang, W. Huang, *ChemCatChem* 5 (2013) 3610–3620.